

# Reproducibility of 3DCRT Isodose Curves Evaluation Obtained Using Spherical Fricke Xylenol Gel Phantom

Christianne C. Cavinato<sup>1</sup>, Benedito H. Souza<sup>2</sup>, Henrique Carrete Jr.<sup>2</sup>, Kellen A. C. Daros<sup>2</sup>, Regina B. Medeiros<sup>2</sup>, Adelmo J. Giordani<sup>3</sup>, Orlando Rodrigues Jr.<sup>1</sup> and Leticia L. Campos<sup>1\*</sup>

<sup>1</sup>Instituto de Pesquisas Energéticas e Nucleares, Gerência de Metrologia das Radiações  
Av. Prof. Lineu Prestes, 2242, 05508-000, São Paulo, Brazil

<sup>2</sup>Universidade Federal de São Paulo, Departamento de Diagnóstico por Imagens  
Rua Napoleão de Barros, 800, 04024-002, São Paulo, Brazil

<sup>3</sup>Universidade Federal de São Paulo, Unidade de Radioterapia  
Rua Napoleão de Barros, 715, 04024-002, São Paulo, Brazil

## Abstract

In this study, in order to evaluate the reproducibility of 3DCRT photon beam isodose curves determination using Fricke xylenol gel (FXG) dosimetry, the isodose curves were obtained from image slices obtained, employing magnetic resonance imaging (MRI) evaluation technique, of different spherical FXG phantoms prepared using 270 Bloom gelatine from porcine skin (made in Brazil). The MRI and optical calibration curves were obtained and the percentage of the dose at specific reference point of different MRI image slices, obtained from FXG phantoms, was calculated. Good qualitative reproducibility in obtaining MRI images of spherical FXG phantoms can be obtained aiming use these results to calculate the isodose curves and the percentage of the dose, to confirm the treatment planning.

**Key Words:** Spherical FXG phantom; 3DCRT; clinical photon beams; magnetic resonance imaging; isodose curves.

## 1 Introduction

For an effective quality control of complex radiation treatment techniques, such as three-dimensional conformal radiation therapy (3DCRT) and intensity modulated radiation therapy (IMRT), is necessary to perform the absorbed dose distribution verification, aiming to confirm that the target volume received the prescribed radiation dose and the healthy tissues surrounding were spared of the ionizing radiation effects (Palta *et al* 2008, Doran 2009). The planar representation of the dose distribution is offered by isodose curves which can be measured in water phantom directly, for example. Isodose curves are lines that join points of equal dose and are used to evaluate treatment plans along a single plane or over several planes in the patient (Podgorsak 2005).

The High Doses Laboratory (LDA) of IPEN developed a Fricke xylenol gel (FXG) using 270 Bloom gelatine from porcine skin (made in Brazil) and has been intensively studied its properties and application, using both spectrophotometry and magnetic resonance imaging (MRI) techniques aiming to use this material to three-dimensional dosimetry applied to radiotherapy and radiosurgery (Cavinato 2009, Cavinato *et al* 2011a, Cavinato *et al* 2011b).

In this study, in order to evaluate the reproducibility of 3DCRT photon beam isodose curves determination using FXG dosimetry, the isodose curves were obtained from images slices obtained

---

\* Presenting author, E-mail: lcredri@ipen.br

employing MRI evaluation technique of different spherical FXG phantoms prepared using 270 Bloom gelatine.

## 2 Materials and Methods

The FXG phantoms and samples were prepared at LDA/IPEN. The gamma and photon irradiations were carried out in the Radiotherapy Service of the Sao Paulo Hospital (HSP) of UNIFESP, the magnetic resonance images were achieved in the Resonance Magnetic Service at Diagnostic Image Department of HSP/UNIFESP, and the optical absorption measures at LDA/IPEN.

### 2.1 Spherical FXG Phantoms and Samples Preparation

For obtaining the spherical FXG phantoms, two spherical glass balloons of 2000 mL (156.0 mm internal diameter and 2.0 mm wall thickness), with one short and thick neck (32.0 mm height, 137.0 mm external diameter, 102.0 mm internal diameter and 17.5 mm wall thickness), were completely filled with a FXG solution prepared (according to Olsson (1989)) on different days to be irradiated and evaluated. The chemical composition of the FXG solution is as follows: 5% by weight 270 Bloom gelatine from porcine skin, ultra-pure water, 50 mM sulphuric acid ( $\text{H}_2\text{SO}_4$ ), 1 mM sodium chloride (NaCl), 1 mM ferrous ammonium sulphate hexahydrate or Mohr's salt [ $\text{Fe}(\text{NH}_4)_2(\text{SO}_4)_2 \cdot 6\text{H}_2\text{O}$ ] and 0.1 mM ferric ions indicator xylene orange ( $\text{C}_{31}\text{H}_{28}\text{N}_2\text{Na}_4\text{O}_{13}\text{S}$ ).

In order to obtain the calibration curves, polymethylmethacrylate (PMMA) cuvettes ( $10 \times 10 \times 45 \text{ mm}^3$ ) were filled with FXG solution. Sets of three samples each were prepared and packed with polyvinyl chloride (PVC) film to prevent evaporation of the water contained in the FXG solution and to ensure the reproducibility of the dosimetric response of the three FXG samples.

The FXG phantoms and PMMA cuvettes were maintained under low temperature ( $(4 \pm 1)^\circ\text{C}$ ) and light protected during about 12 hours after preparation. The FXG phantoms were positioned in a Styrofoam box containing ice cubes in order to keep them under low temperature and light protected to be transported to the irradiation site.

### 2.2 Treatment Planning

Computed tomography (CT) scans were obtained from a similar spherical glass flask used to FXG phantom preparation, in this case, completely filled with tri-distilled water, using a Philips® Brilliance CT 64-channel scanner (HSP/UNIFESP). The 3D treatment planning (in sagittal and axial CT slices) was performed using the Eclipse® External Beam Planning system version 7.3.10 (figure 1). Multiple static radiation fields were used and the irradiation parameters are presented in table 1.

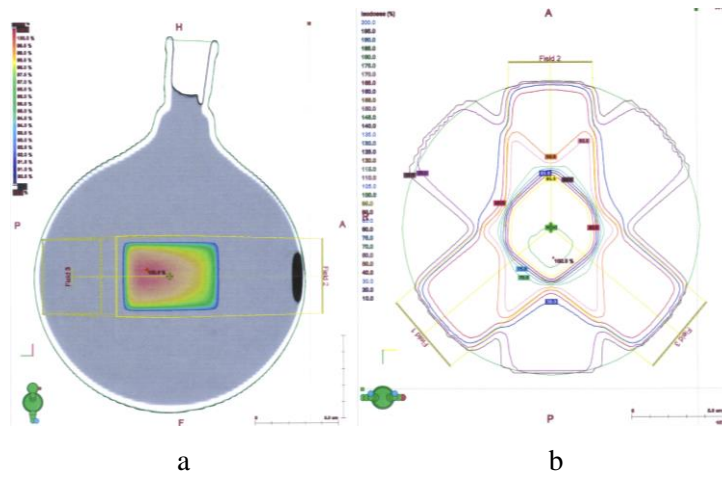


**Figure 1.** Three-dimensional treatment planning (Eclipse® External Beam Planning system) in sagittal (a) and axial (b) CT slices for spherical FXG phantoms irradiations.

**Table 1.** Irradiation parameters for the FXG phantoms.

Radiation Field	Gantry Position (°)	Treatment Couch Position (°)	Field Size (cm)				SSD (cm)	Monitor Unit (MU)
			X1	X2	Y1	Y2		
1	230.0	0.0	+ 2.5	+ 2.5	+ 2.5	+ 2.5	91.9	853
2	0.0	0.0	+ 2.5	+ 2.5	+ 2.5	+ 2.5	91.9	854
3	130.0	0.0	+ 2.5	+ 2.5	+ 2.5	+ 2.5	91.9	854

## 2.3 Irradiations

The spherical FXG phantoms and PMMA cuvettes were maintained at room temperature and light protected during about 30 minutes before irradiation.

### 2.3.1 FXG Samples

The PMMA cuvettes filled with FXG solution were positioned at source-surface distance (SSD) of 80 cm in a PMMA plates phantom (build-up and backscattering PMMA plates 1.5 cm thick) and irradiated with different photon doses ranging from 2 to 30 Gy, dose rate of 74.98 cGy.min<sup>-1</sup>, 40 x 40 cm<sup>2</sup> field size, using a GENERAL ELECTRIC COMPANY® Alcyon II <sup>60</sup>Co gamma radiation machine (HSP/UNIFESP). These FXG samples were irradiated with <sup>60</sup>Co gamma radiation considering the homogeneity and precision of absorbed dose delivery of <sup>60</sup>Co gamma sources and that the effective photon energy of 6 MV photon beam is approximately 2 MeV.

All FXG sample sets were positioned together in the PMMA phantom and each set was removed when the radiation exposure time needed to obtain the desired absorbed dose was completed.

### 2.3.2 Spherical FXG Phantoms

The spherical FXG phantoms irradiations were housed in a foam backer to be irradiated with 6 MV clinical photon beams, absorbed dose of 20 Gy and dose rate of 300 cGy.min<sup>-1</sup>, using a

VARIAN® Clinac 600C linear accelerator (HSP/UNIFESP). The irradiation parameters presented in table 1 also were used.

The experimental set up for spherical FXG phantoms irradiations with clinical photon beams is presented in figure 2.

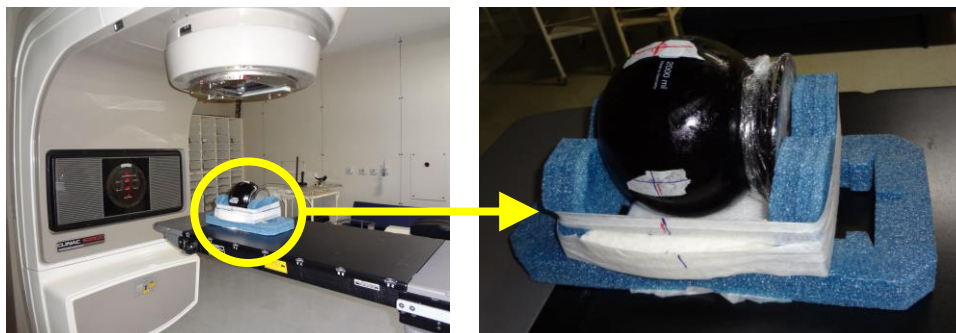


**Figure 2.** Experimental set up for spherical FXG phantoms irradiations with clinical photon beams.

## 2.4 Evaluation

The MRI technique was used for obtaining images of FXG phantoms and PMMA cuvettes, which were acquired about 30 minutes after irradiation, using a SIEMENS® MAGNETOM® Sonata Maestro Class 1.5 T MRI scanner (HSP/UNIFESP), on cranium protocol-T1. The MRI images acquisition parameters are presented in table 2. In order to process the MRI scans obtained, the softwares syngo fastView® version VX57F24 and ImageJ® version 1.42q were used.

**Table 2.** MRI images acquisition parameters.

<i>Parameters Description</i>	<i>Values</i>
Image Orientation	Coronal, sagittal and axial
Field of View (FOV) (mm)	256
Slice Thickness (THK) (mm)	3.0
Voxel (mm)	1.0 x 1.0 x 1.0
Gap (mm)	3.0
Time of Repetition (TR) (ms)	2000
Time of Echo (TE) (ms)	3.42
Flip Angle (°)	15
Matrix Size (MS) (pixels)	256 x 256
Number of Signals Averaged (NSA)	1
Slices Number	41
Coil	Head
Channels	8

The PMMA cuvettes were also evaluated by optical absorption (OA) spectrophotometry technique to compare the obtained results, using a SHIMADZU® UV2101-PC spectrophotometer (wavelength range from 190 to 900 nm) of LDA/IPEN.

The MRI and OA calibration curves were obtained and the absorbance values presented correspond to dosimetric wavelength of 585 nm (Bero 2001). Each presented value corresponds to the

average of the measurement of three samples and the error bars the standard deviation of the mean. The background values corresponding to the magnetic and optical measurements of non-irradiated Fricke gel samples were subtracted from all values presented.

The percentage of the dose at specific reference point of different MRI images slices obtained from FXG phantoms was calculated. The Python scripts were used for postprocessing the following tasks: identifying of the information in DICOM files and calibration curve fitting. The images were generated using custom software written in MATLAB.

### 3 Results and Discussion

#### 3.1 Calibration Curves

The MRI images (coronal orientation) of the PMMA cuvettes filled with FXG solution, irradiated with  $^{60}\text{Co}$  gamma radiation (dose range from 2 to 30 Gy) is presented in figure 3.

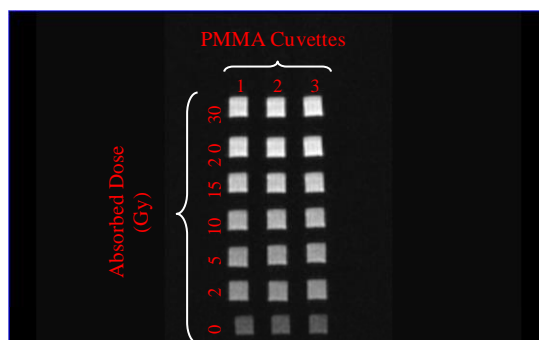


**Figure 3.** Coronal MRI images of the FXG solution conditioned in PMMA cuvettes, non-irradiated and irradiated with  $^{60}\text{Co}$  gamma radiation.

The MRI and OA calibration curves are presented in figure 4. The MRI signal intensity (figure 4(a)) was obtained from figure 3.

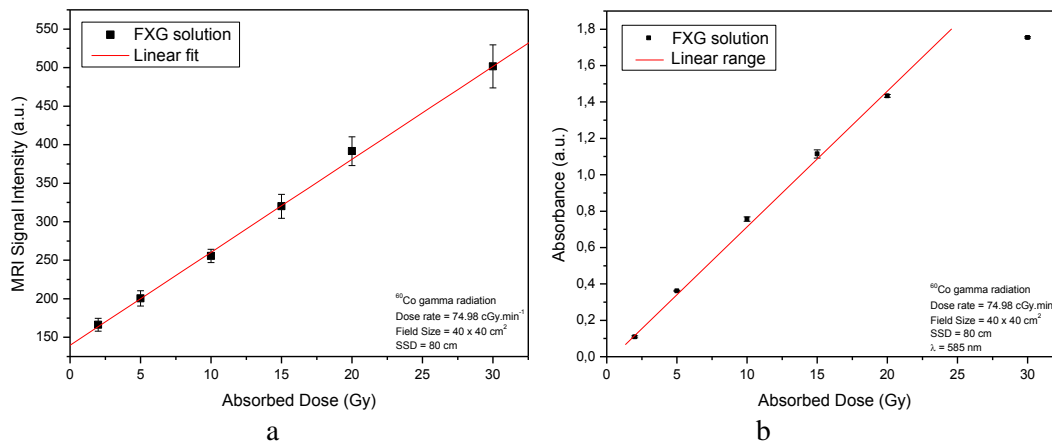


**Figure 4.** MRI signal intensity curve in function of absorbed dose (a) and optical dose-response curve (b) of the FXG solution irradiated with  $^{60}\text{Co}$  gamma radiation.

The FXG solution response in function of absorbed dose presents linear behavior in the clinical interest dose range (2 to 20 Gy) for both evaluation techniques, tending to saturation to doses equal and higher than 20 Gy (AO technique). The optical dose-response curve was obtained only as reference system.

### 3.2 FXG Phantoms MRI Images

In figure 5 are presented the MRI images slices, in sagittal, coronal and axial orientations, of the spherical FXG phantom non-irradiated and irradiated (6 MV photons and 20 Gy).

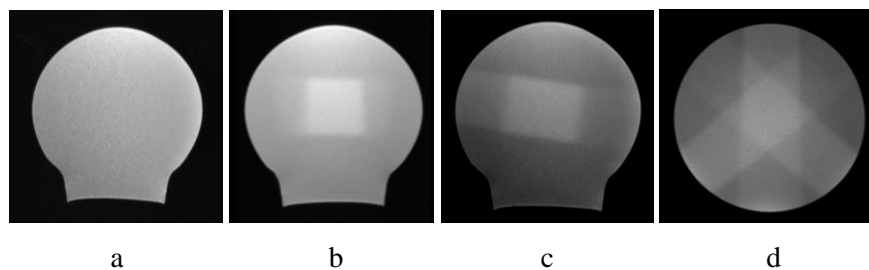


**Figure 5.** Sagittal MRI image slice of non-irradiated spherical FXG phantom (a). Coronal (b), sagittal (c) and axial (d) MRI images slices of the FXG phantom irradiated with 6 MV photons.

It is clearly possible to observe the target volume irradiated in the MRI images slices in different orientations (coronal, sagittal and axial) and in the axial image slice (figure 5(d)), can also be seen the input and the overlap of multiple radiation fields.

The MRI images slices of two different spherical FXG phantoms irradiated, in sagittal and axial orientations, are presented in figures 6 and 7, respectively.

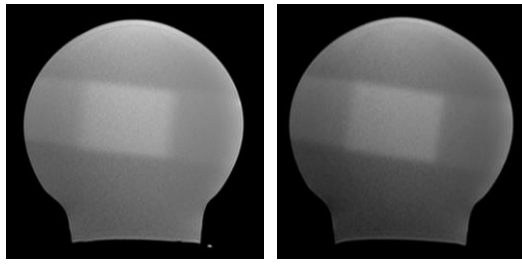


**Figure 6.** Sagittal MRI images slices of different spherical FXG phantoms irradiated with 6 MV photons.

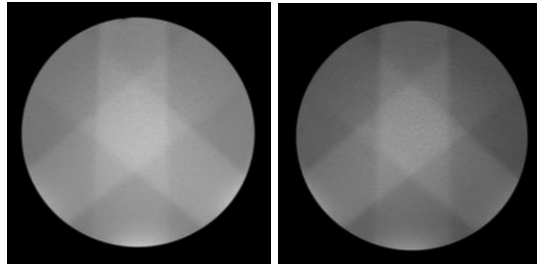


**Figure 7.** Axial MRI images slices of different spherical FXG phantoms irradiated with 6 MV photons.

A good qualitative reproducibility of the MRI images slices of two FXG phantoms, in different orientations can be observed.

### 3.3 Isodose Curves and 3D MRI Slice Reconstruction

Isodose curves calculated in percentage of the dose for sagittal and axial MRI slices of different spherical FXG phantoms irradiated (6 MV photons) are presented in figures 8 and 9, respectively.

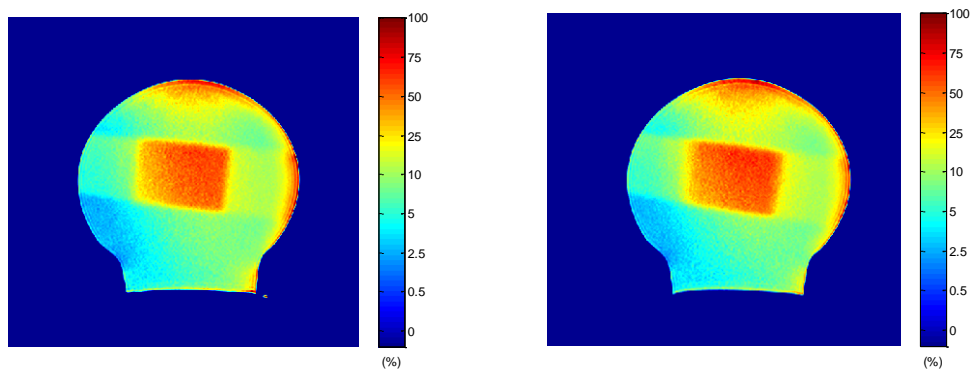


**Figure 8.** Isodose curves calculated for sagittal MRI slices of two FXG phantoms irradiated with 6 MV photons.

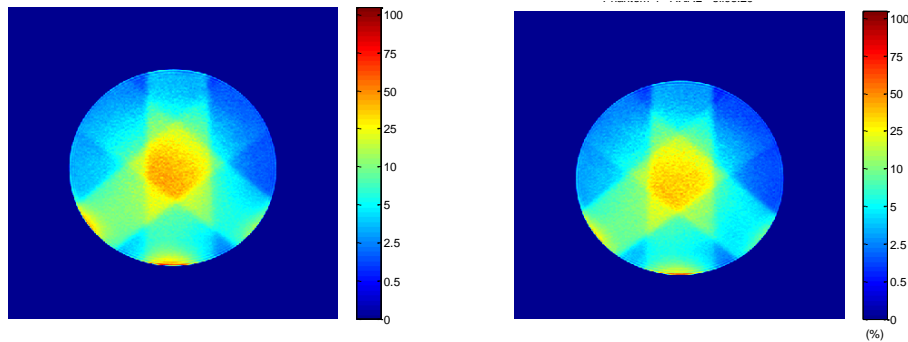


**Figure 9.** Isodose curves calculated for axial MRI slices of two FXG phantoms irradiated with 6 MV photons.

Three-dimensional axial MRI slice reconstruction of the spherical FXG phantom irradiated with 6 MV photons is presented in figure 10.

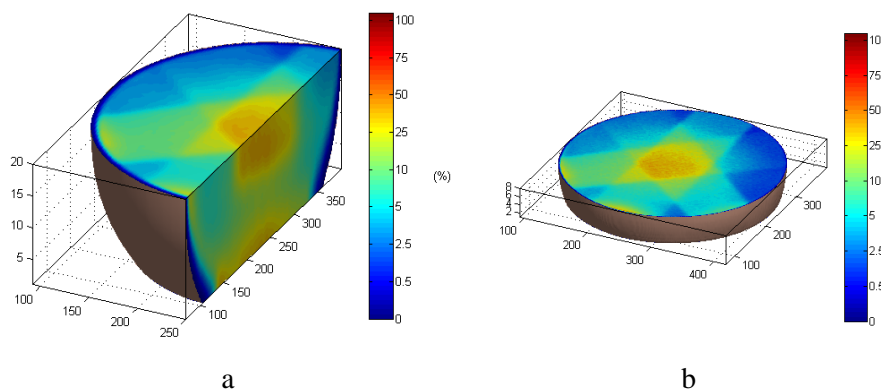


**Figure 10.** Three-dimensional axial MRI slice reconstruction: 40 slices (cuts in xSlice = 250/zSlice = 20) (a); 1 slice (cut in zSlice = 8) (b).

In all figures (8, 9, 10) clearly can be seen that the target volume received the highest percentage of the dose and the overlap of multiple static radiation fields and their projections.

#### 4 Conclusions

Good qualitative reproducibility in obtaining MRI images of spherical FXG phantoms (prepared with 270 Bloom gelatine, made in Brazil) can be obtained aiming use these results to calculate the isodose curves and the percentage of the dose, to confirm the treatment planning.

#### Acknowledgements

The authors are grateful to the staffs of the Radiotherapy Service and Resonance Magnetic Service of the Diagnostic Image Department of the HSP/UNIFESP to allow the FXG irradiations and MR evaluations, respectively, and CAPES, FAPESP, CNPq, IPEN, CNEN, MCT: Project INCT for



Radiation Metrology in Medicine and MRA Indústria de Equipamentos Eletrônicos Ltda. by the financial support.

## References

Bero M.A., Gilboy W.B., Glover P.M., 2001, Radiation in Physics and Chemical, 433-435.

Cavinato C.C., 2009, Padronização do Método de Dosimetria Fricke Gel e Avaliação Tridimensional de Dose Empregando a Técnica de Imageamento por Ressonância Magnética, São Paulo, Instituto de Pesquisas Energéticas e Nucleares.

Cavinato C.C., Sakuraba R.K., Cruz J.C., Campos L.L., 2011a, Radiation Measurements, 1928-1931.

Cavinato C.C., Souza B.H., Carrete Jr. H., Daros K.A.C., Medeiros R.B., Giordani A.J., Campos L.L., 2011b, Revista Brasileira de Física Médica, 5(2), 133-138.

Doran S.J., 2009, Applied Radiation and Isotopes, 393-398.

Olsson L.E., Petersson S., Ahlgren L., Mattsson, S., 1989, Physics in Medicine and Biology, 43-52.

Palta J.R., Liu C., Li J.G., 2008, International Journal of Radiation Oncology Biology Physics, S108-S112.

Podgorsak EB., 2005, Radiation Oncology Physics: a handbook for teachers and students, Vienna, International Atomic Energy Agency.